Development of prostate specific membrane antigen targeted ultrasound microbubbles using bioorthogonal chemistry

Aimen Zlitni[1¤], Melissa Yin[2], Nancy Janzen[1], Samit Chatterjee[3], Ala Lisok[3], Kathleen L. Gabrielson[3], Sridhar Nimmagadda[3], Martin G. Pomper[3], F. Stuart Foster[2]*, John F. Valliant[1,4]*

1 Department of Chemistry and Chemical Biology, McMaster University, Hamilton, Ontario, Canada, **2** Department of Medical Biophysics, University of Toronto, Toronto, Ontario, Canada, **3** Russell H. Morgan Department of Radiology and Radiological Science, Johns Hopkins Medical Institutions, Baltimore, Maryland, United States of America, **4** Centre for Probe Development and Commercialization, Hamilton, Ontario, Canada

¤ Current address: Department of Radiology, Stanford University, Stanford, California, United States of America.
* valliant@mcmaster.ca (JFV); stuart@sri.utoronto.ca (FSF)

Abstract

Prostate specific membrane antigen (PSMA) targeted microbubbles (MBs) were developed using bioorthogonal chemistry. Streptavidin-labeled MBs were treated with a biotinylated tetrazine (MB_{Tz}) and targeted to PSMA expressing cells using *trans*-cyclooctene (TCO)-functionalized anti-PSMA antibodies (TCO-anti-PSMA). The extent of MB binding to PSMA positive cells for two different targeting strategies was determined using an *in vitro* flow chamber. The initial approach involved pretargeting, where TCO-anti-PSMA was first incubated with PSMA expressing cells and followed by MB_{Tz}, which subsequently showed a 2.8 fold increase in the number of bound MBs compared to experiments performed in the absence of TCO-anti-PSMA. Using direct targeting, where TCO-anti-PSMA was linked to MB_{Tz} prior to initiation of the assay, a 5-fold increase in binding compared to controls was observed. The direct targeting approach was subsequently evaluated *in vivo* using a human xenograft tumor model and two different PSMA-targeting antibodies. The US signal enhancements observed were 1.6- and 5.9-fold greater than that for non-targeted MBs. The lead construct was also evaluated in a head-to-head study using mice bearing both PSMA positive or negative tumors in separate limbs. The human PSMA expressing tumors exhibited a 2-fold higher US signal compared to those tumors deficient in human PSMA. The results demonstrate both the feasibility of preparing PSMA-targeted MBs and the benefits of using bioorthogonal chemistry to create targeted US probes.

Introduction

Prostate cancer (PCa) is the second leading cause of cancer-related deaths in men [1]. It is estimated that in 2015 more than 220,000 people in the USA and 24,000 in Canada were diagnosed

with PCa, which would account for 26% of all new cancer cases in men [1,2]. When detected early, the 5-year survival rate is around 99%. However, survival drops dramatically once the cancer has spread beyond the prostate [3]. The gold standard for PCa diagnosis is trans-rectal ultrasound (TRUS)-guided biopsies from patients with elevated serum levels of prostate specific antigen. Unfortunately, TRUS biopsies have a high rate of false-negative results often leading to repeat biopsy procedures [4–7]. While ultrasound (US) imaging of PCa is used routinely, its role in visualizing focal lesions is limited by the lack of targeted imaging [8]. This is driving the need for PCa-targeted US contrast agents to enhance the sensitivity and accuracy of US in detecting malignant masses both during diagnosis and following the initiation of therapy [9]. Such a technique would help improve diagnostic sensitivity and specificity, help support active surveillance strategies and reduce the need for repeat biopsies [9]. Although recent work has indicated that magnetic resonance imaging (MRI) guided biopsy may be superior to TRUS in detection of clinically significant PCa [10], the availability, portability and relative low cost of US make it an attractive tool for active surveillance of PCa particularly when combined with targeted contrast agents.

One approach to improving PCa detection is to employ imaging agents that target prostate specific membrane antigen (PSMA). PSMA is a transmembrane glycoprotein that is expressed at low levels in normal prostate, liver, kidney and brain tissue, but is expressed at much higher levels in PCa tumors [11–17]. High PSMA expression correlates with pathological stage and tumor grade, and was demonstrated as an independent predictor of biochemical recurrence [18,19]. Agents for visualizing PSMA with nuclear imaging methods such as positron emission tomography (PET) include both radiolabeled small molecules and antibodies, which have been used clinically in patients with both primary and metastatic disease [20–30]. Results from these studies support the use of PSMA as a PCa biomarker.

A microbubble based (MB) contrast agent that targets PSMA would provide the opportunity to use US imaging to detect and characterize primary and recurrent PCa [31]. PSMA is highly expressed on the endothelial cells in the microvasculature of prostate tumors making it a suitable target for molecular US imaging using targeted MBs, which are generally restricted to targets within the vasculature due to their size [32]. A PSMA-targeted US method could be used for detecting PCa lesions and for biopsy guidance, offering a way to improve existing non-contrast enhanced US techniques, while also providing an alternative to more costly and time consuming MRI-based biopsy guidance methods [33].

Sanna and coworkers prepared polymer-based MBs covalently attached to a small-molecule inhibitor of PSMA [34]. The MBs showed specific binding to PSMA-expressing (PSMA$^+$) cells *in vitro*, however the evaluation of this agent under dynamic flow conditions or in preclinical animal models has not yet been reported. Wang and coworkers prepared nano-scale US contrast bubbles (NBs) coated with streptavidin and loaded with a biotinylated derivative of an anti-PSMA antibody [35]. *In vitro* and *in vivo* studies showed a statistically significant but modest difference in the binding of the PSMA-targeted NBs, where the ratio of the US signal obtained from targeted compared to non-targeted NBs was less than 1.20. These researchers also targeted the same NBs using a biotinylated derivative of an anti-PSMA nanobody, which showed similar binding compared to the anti-PSMA antibody [36]. Although this prior work indicates targeting to PSMA may be feasible, it is clear that the type of targeting agent and the nature of its linkage to the US contrast agent is critical and have not been fully optimized. Furthermore, the methods used to produce the PSMA-targeted MBs should be readily accessible to the scientific community and the associated chemistry adaptable for producing MBs that can be used in clinical studies.

Here we utilize the high yielding, selective and rapid bioorthogonal chemical reaction between tetrazine (Tz) and *trans*-cyclooctene (TCO) to create PSMA binding MBs (Fig 1A)
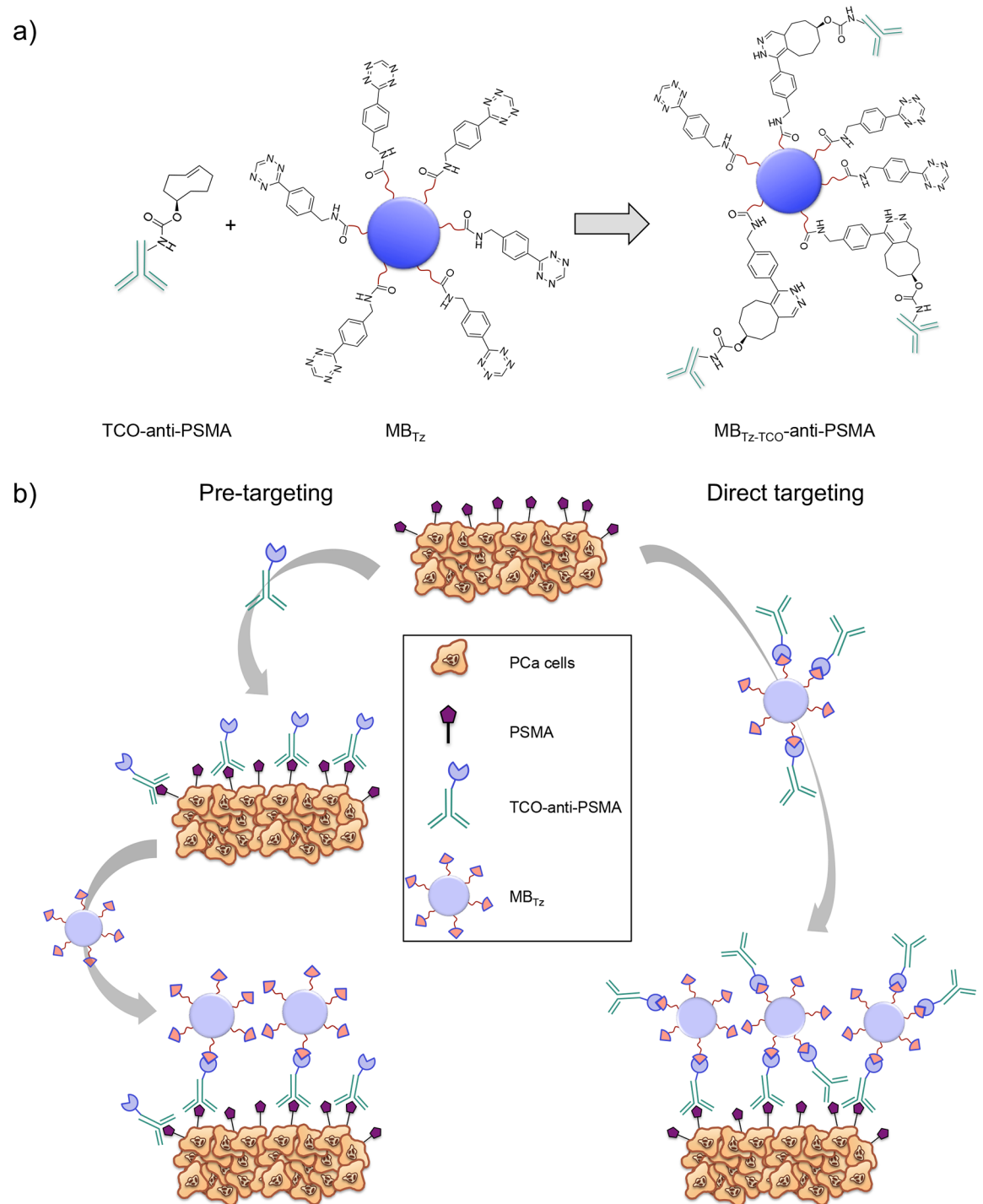
Fig 1. Cycloaddition reaction and targeting strategies for MB$_{Tz}$. a) Schematic illustrating the cycloaddition reaction between tetrazine functionalized microbubbles (MB$_{Tz}$) and *trans*-cyclooctene (TCO)-conjugated PSMA antibody (TCO-anti-PSMA) producing targeted MBs (MB$_{Tz-TCO}$-anti-PSMA). b) Schematic representation of the two strategies used to target MB$_{Tz}$ to PSMA-expressing PCa cells. Right: MB$_{Tz}$ is treated with TCO-anti-PSMA (MB$_{Tz-TCO}$-anti-PSMA) before injection (direct targeting). Left: TCO-anti-PSMA is injected first and allowed to bind to PSMA-expressing cells and clear non-targeted tissue before injecting MB$_{Tz}$ (pretargeting).

https://doi.org/10.1371/journal.pone.0176958.g001

[37]. This methodology has been used successfully to target MBs to the angiogenesis marker vascular endothelial growth factor receptor 2 (VEGFR2) [37] where the use of bioorthogonal chemistry affords the opportunity to employ two different approaches for targeting MBs to the biomarker of interest (Fig 1B). The first is a direct targeting strategy, which involves ligating a target-specific, TCO-labeled antibody (TCO-anti-PSMA) with Tz-functionalized MBs (MB$_{Tz}$) creating antibody-targeted MBs (Fig 1A), prior to administration and US imaging. The second is a pretargeting strategy, in which the TCO-labeled antibody is administered first, to allow binding to sites of target antigen overexpression and clearance from non-target organs. This is followed by injection of MB$_{Tz}$ that will selectively react with target-bound TCO-anti-PSMA *in vivo*. While the former has the advantage of simplicity, the latter eliminates the influence of the large size of the MB on the ability of the antibody to bind the target. We report here the development and evaluation of both approaches and demonstrate US imaging of PSMA-expressing tumors *in vivo*.

Materials and methods

General materials and instruments

Microbubbles (MBs) were obtained (8.4×10^8 MBs/vial) from a MicroMarker^{TM}, Target-Ready Contrast Agent Kit (VisualSonics Inc., Toronto, ON). Streptavidin coated magnetic beads (New England BioLabs, Whitby, ON) and MACSiMAG^{TM} separator magnet (Miltenyi Biotec, Auburn, CA) were used during the purification of MBs. Conjugated antibodies were analyzed by mass spectrometry on a MALDI Bruker Ultraflextreme Spectrometer. MB size and concentration were determined using Z2 Coulter counter (Beckman Coulter, Fullerton CA). The syringe pump used in the flow chamber assay was a PhD 2000 (Harvard Apparatus, Holliston, MA). Western blot images were generated using a STORM 840 imaging system (GMI Ltd., Ramsey, MN)

Preparation of TCO-modified antibodies

J591, an anti-PSMA monoclonal antibody (mAb) that binds the extracellular domain of human PSMA [38], was provided by Dr. Neil Bander (Department of Urology, Cornell University), where TCO-modified J591 was prepared following a modified literature method [37]. Briefly, the pH of a solution of J591 antibody (500 µL, 250 µg, 1.67 nmol) in PBS was adjusted to 9 by adding 3 µL of 1 M Na$_2$CO$_3$ (aq). (*E*)-Cyclooct-4-enyl-2,5-dioxopyrrolidin-1-yl carbonate (TCO-NHS) was then added (17.8 µg, 66.8 nmol, 40 eq) in 9 µL of DMSO. The solution was left on a shaker overnight at 4°C. The desired product (TCO-J591) was isolated from excess TCO using an Amicon Ultra-0.5 Centrifugal filter (30 kDa) and washed with PBS three times. Matrix-Assisted Laser Desorption Ionization Time-of-Flight Mass Spectrometry (MALDI-TOF MS) analysis of the antibody, before and after conjugation to TCO, showed an average of 1.2 TCO groups per antibody using a MALDI Bruker Ultraflextreme Spectrometer (S1 File). TCO was added to a second PSMA binding antibody (ARP44691_p050; Aviva Systems Biology, San Diego, CA) following the same method where the product is referred to herein as TCO-ARP.

Synthesis of biotin-Tz

N-(4-(1,2,4,5-Tetrazin-3-yl)benzyl)-6-(5-((4*S*)-2-oxohexahydro-1*H*-thieno[3,4-*d*]imidazol-4-yl)pentanamido)hexanamide (biotin-Tz) was synthesized as previously described [37]. The structure of biotin-Tz is shown in S2 File.

Preparation of tetrazine-functionalized microbubbles (MB$_{Tz}$)

Streptavidin-coated MBs (MicroMarker^{TM}; VisualSonics Inc.) were reconstituted in 500 µL sterile saline (0.9% NaCl), according to the manufacturer's instructions. To prepare MB$_{Tz}$, biotin-Tz (70 µg, 1.35×10^{-4} mmol) in 50 µL of saline:methanol (1:1 v/v) was added dropwise to the reconstituted MBs. After 45 min, 200 µL from the bottom of the vial was removed carefully with minimal agitation and was discarded. Then, a 200 µL suspension of streptavidin-coated magnetic beads (New England BioLabs) were added and the solution set aside for 20 min. Thereafter, 200 µL of the solution was removed carefully and discarded, and the remaining mixture was placed beside a MACSiMAG^{TM} magnet (Miltenyi Biotec) to remove any residual magnetic bead-bound biotin-Tz. Saline (200 µL) was then added to MBs and the solution transferred to another vial. MBs size and concentration were determined using Z2 Coulter counter (Beckman Coulter).

Preparation of anti-PSMA antibody coated MBs

Anti-PSMA coated MBs were prepared by combining MB$_{Tz}$ with either TCO-J591 or TCO-ARP. Briefly, a MB$_{Tz}$ solution (50 µL, 3×10^7 MBs for *in vitro* studies; 120 µL, 7×10^7 MBs for *in vivo* studies) was mixed with the TCO-anti-PSMA antibody (20 µL/10 µg for *in vitro* studies; 50 µL/ 25 µg for *in vivo* studies). The reaction was allowed to proceed for 20 min at room temperature. The resulting constructs MB$_{Tz\text{-}TCO}$-J591 and MB$_{Tz\text{-}TCO}$-ARP were used immediately for *in vitro* binding and *in vivo* imaging studies.

Cell lines and culture methods

PC-3 cells transfected with human PSMA were generously provided by Molecular Insight Pharmaceuticals, Inc. (Cambridge, MA). PC-3 cells were cultured in F12-K media supplemented with 10% FBS, 1% penicillin-streptomycin and 0.1% geneticin. LNCaP cells, derived from lymph node metastases of human prostate carcinoma, were purchased from ATCC (CRL-1740), and cultured in RPMI-1640 Medium supplemented with 10% FBS and 1% penicillin-streptomycin. The cell lines were maintained at 37˚C under 5% CO_2.

Flow chamber assay

The flow assay was performed as previously described [37]. Briefly, 8×10^5 of PC-3 cells were plated separately in 30 mm Corning tissue culture dishes, 2 days prior to running the assay. The setup of the parallel-plate flow chamber (Glycotech, Rockville, MD) is shown in S3 File. In the pretargeting strategy and associated controls, cells were incubated first with TCO-J591 (30 µg/mL) for 30 min. For direct targeting, TCO-J591 was incubated with MB$_{Tz}$ for 20 min. creating the targeted MBs (MB$_{Tz\text{-}TCO}$-J591) that were subsequently used in the flow assay. Using a syringe pump, cells were first rinsed with 1 mL of PBS, and then 1 mL of MB solution at a shear rate of 100 sec^{-1} (flow rate = 0.164 mL/min). Thereafter, the plate was rinsed with 2 mL of PBS at a shear rate of 1000 sec^{-1}. Binding of MBs was visualized using a Celestron Penta-View LCD Digital Brightfield S4 Microscope with 20× objective. Images were recorded and the extent of binding was assessed by comparing the area covered by MBs to the total area covered by cells in each image using image analysis (FIJI) software [37,39].

Mouse xenograft tumor model and procedures

All research that involved in vivo study in mice was done with the approval of Institutional Animal Care and Use Committees at McMaster University (Animal Research Ethics Board), Sunnybrook Research Institute (SRI Animal Care Committee), and Johns Hopkins Medical

(Animal Care and Use Committee). Mice were maintained with 12 h light/dark cycles and given food and water *ad libitum*. The human prostate carcinoma LNCaP cells were used to provide xenograft tumors. NCr nude male mice (4 to 5 week old) were purchased (Taconic Labs, Germantown, NY) and were injected with 2.0×10^6 LNCaP cells in 100 μL Matrigel/ DPBS (1:1; VWR-Canlab, Mississauga, ON and Invitrogen, Burlington, ON) subcutaneously in the right flank. To isolate tumor tissue, mice were sacrificed by cervical dislocation immediately following imaging, and the tumors excised, rinsed with PBS and frozen in liquid N_2. Frozen tumors were stored at -80˚C. Animal studies involving PC-3 cells utilized human prostate cancer PC-3 cells transfected to overexpress PSMA (PSMA⁺) or transfected with the plasmid alone (PSMA⁻) were implanted subcutaneously in severe-combined immunodeficient (SCID) mice (Johns Hopkins Immune Compromised Animal Core) at the forward right and left flank respectively, as previously reported [40].

Tumor lysate preparation

Each frozen tumor was thawed and put into lysis buffer containing 1% IGEPAL CA-630 (I3021; Sigma-Aldrich, Oakville, ON), 20mM Tris pH 8.0 (154563; Sigma-Aldrich), 137mM NaCl (S6191; Sigma-Aldrich), 10% glycerol (5350–1; Caledon Laboratories), 2mM EDTA (E5134; Sigma-Aldrich) and Protease Inhibitor cocktail (PIC003; Bioshop Canada, Burlington, ON). Each tumor was subsequently homogenized using VWR PowerMax AHS 200 homogenizer (5×75 mL troemner) and lysate collected after centrifugation ($2000 \times g$, 5 min) and washing three times with PBS. Protein concentration was determined using a Pierce® BCA Protein Assay Kit (ThermoFisher Scientific, Ottawa, ON).

Western blot analysis of cell lysates

Using immunoblotting, PSMA protein expression by PSMA⁺ LNCaP and transfected PSMA⁺ PC-3 cells was assessed and compared to PSMA⁻ PC-3 cells. 10 μg of protein from each cell lysate were loaded on 10% Mini-PROTEAN TGX precast gels and fractionated by SDS-PAGE. After electro-transferring the protein extracts to polyvinylidene difluoride (PVDF) membrane, the membrane was incubated with PSMA antibody (E-18), a goat polyclonal antibody (sc-10269; Santa Cruz Biotechnology, Dallas, TX), specific for mouse and human PSMA, in a 1:250 dilution overnight at 4˚C. After washing, the membrane was incubated with AP-Bovine anti-goat IgG antibody (sc-2351; Santa Cruz Biotechnology) in a 1:2000 dilution for 1 h at room temperature. The membrane was then washed and incubated with a chemiluminescent reagent (ECF substrate, GE RPN5785) for 5 min and imaged using a STORM 840 system (GMI Ltd., Charlotte, NC).

Western blot analysis of tumor lysates

PSMA expression by LNCaP tumors used in imaging studies was assessed by immunoblotting. Tumor lysates were loaded on 10% Mini-PROTEAN TGX precast gels and fractionated by SDS-PAGE. Protein extracts were electro-transferred to PVDF membrane. The PVDF membrane was incubated with PSMA (E-18) goat anti-PSMA antibody (sc-10269; Santa Cruz Biotechnology) in a 1:250 dilution, and anti-β-Actin (13E5) rabbit mAb (4970; Cell Signaling Technology, Beverly, MA) in a 1:2000 dilution overnight at 4˚C. The membrane was then washed and incubated with AP-Bovine anti-goat IgG (sc-2351; Santa Cruz Biotechnology) plus AP-Goat anti-rabbit IgG (H+L) (111055045, Jackson ImmunoResearch) in a 1:2000 dilution for 1 h at room temperature. Finally, the membrane was washed and incubated with a chemiluminescent reagent (ECF substrate, GE RPN5785) for 5 min and imaged using a

STORM 840 imaging system (GMI Ltd.). Bands for PSMA and ß-actin were quantified using ImageQuant TL software (GE Healthcare Life Sciences).

Ultrasound imaging and analysis

Using a Vevo®2100 imaging system (VisualSonics) and a 20 MHz high-frequency solid-state transducer (MS-250; VisualSonics), LNCaP tumor-bearing mice were imaged using non-linear contrast mode. Animals were kept under anesthesia using isoflurane (4% initiation, 2% maintenance) during the imaging session. MBs were administered in a 70 μL bolus (approximately $5–6 \times 10^7$ MBs) via the tail vein, using a syringe pump at a 600 μL/min injection rate. Each mouse was first injected and imaged with MB_{Tz} alone as a control, followed by a *circa* 15 min delay for the MBs to clear. This was followed by a second injection of MB_{Tz} that had been coupled to the TCO-anti-PSMA antibody. After each injection, MBs were allowed to circulate for 4 min before initiating a disruption replenishment sequence [41]. Typically 200 frames of images were acquired before initiating a 1 sec high power disruption sequence, followed by another 300 frames of image acquisition. 3D disruption sequences were applied between each injection to establish complete clearance of previously injected MBs.

US imaging studies on $PSMA^+$ and $PSMA^-$ PC-3 tumors were conducted using Vevo®3100 imaging system (VisualSonics) and a 20 MHz high-frequency solid-state transducer (MS-250; VisualSonics) using non-linear contrast mode. MBs targeted to both human and mouse PSMA (MB_{Tz-TCO}-ARP) were administered as stated above and allowed to circulate for 4 min before imaging. In random order, either $PSMA^+$ then $PSMA^-$ tumor models were imaged using a disruption replenishment sequence.

For all studies, the differential targeted enhancement (dTE) signal was measured using a contrast quantification software analysis tool (VevoCQ™, VisualSonics). Regions of interest were determined based on the distribution of the MBs in the tumor (only vascular regions were included) and was kept constant for each animal when evaluating the different MBs. In order to distinguish and quantify the US signal coming from tumor-bound MBs, the average intensity over 200 frames acquired 5 sec after disruption (which represents the US signal coming from circulating MBs) was subtracted from the average intensity over 200 frames acquired before disruption (which represents the US signal coming from tumor-bound and circulating MBs). The signal attributed to tumor-bound MBs is then presented as parametric maps overlaid onto the non-linear contrast US images.

Statistical analysis

Statistical analysis of the data from the flow chamber binding assay and the US imaging was performed by one-way ANOVA. The results for flow chamber binding assay were confirmed post-hoc using the Bonferroni test.

Results and discussion

Preparation of PSMA-targeted MBs

The tetrazine functionalized microbubbles (MB_{Tz}) were prepared by adding *N*-(4-(1,2,4,5-tetrazin-3-yl)benzyl)-6-(5-((4*S*)-2-oxohexahydro-1*H*-thieno[3,4-*d*]imidazol-4-yl)-pentanamido)-hexanamide (biotin-Tz, S2 File) to commercially available streptavidin coated MBs [37]. TCO-labeled anti-PSMA antibodies were prepared by combining the protein with (*E*)-cyclooct-4-enyl-2,5-dioxopyrrolidin-1-yl carbonate (TCO-NHS) at pH 9–9.5 and 4°C overnight. The number of TCO moieties per antibody was 1.2 as determined by MALDI-TOF MS (S1 File). Initial screening studies were performed using J591, which binds to the extracellular domain

of human PSMA [38] and has been shown to be a highly effective tool for targeting radioisotopes and nanomaterials to PSMA expressing tumors [14,38,42–46]. J591 was chosen from among several anti-PSMA mAbs that have been investigated for targeted imaging and targeted radiotherapy [47–52]. J591 has the advantages of being a humanized mAb used in clinical studies [28] and it binds to the extracellular domain of PSMA present on the surface of viable tumor cells [38], rather than targeting the intracellular domain that is accessible only within necrotic regions [53].

In vitro screening of direct and pretargeting of MBs to PSMA

The ability to target MBs to PSMA *in vitro* was assessed in a flow chamber adhesion assay (S3 File). The flow chamber system is designed to provide a more realistic test environment for evaluating the ability of targeted MBs to bind receptors in the dynamic environment found in tumor microvasculature compared to that of a traditional cell culture assays [54]. Although the PSMA$^+$ LNCaP cells were chosen for *in vivo* targeting studies (*vide infra*), they have low adhesive properties in culture, and therefore were not suitable for use in the flow chamber system. Instead, more adherent PC-3 cells that were PSMA$^+$ (human PSMA gene-transfected) or PSMA$^-$ (non-transfected) were used. Western blot analysis of the two PC-3 cell lines showed PSMA protein expression in the PSMA$^+$ PC-3 cells at levels comparable to LNCaP cells, and no expression by PSMA$^-$ PC-3 cells (S4 File).

Both the pretargeting and direct targeting approaches were evaluated using the *in vitro* flow chamber assay. For pretargeting, TCO-J591 was incubated with the PC-3 cells that were then rinsed before introducing MB$_{Tz}$. For direct targeting, TCO-J591 was first incubated with MB$_{Tz}$ creating the targeted MBs (MB$_{Tz-TCO}$-J591). Both the MB$_{Tz}$ (pretargeting) and the MB$_{Tz-TCO}$-J591 conjugates (direct targeting) were added at a standard flow rate. After increasing the flow rates to remove any non-covalently bound MBs, bright-field microscopy images were collected and images were analyzed using FIJI software following a literature procedure [37].

Microscopy images (Fig 2) showed higher binding for both pretargeting and direct targeting compared to what was observed for non-functionalized MBs. Image analysis indicated
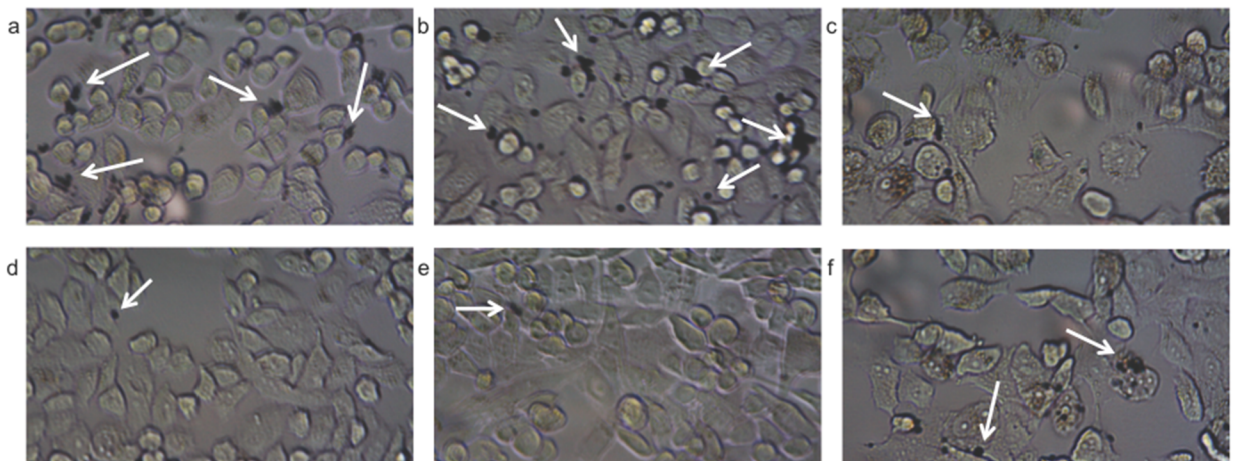
Fig 2. Bright-field microscopy of MB$_{Tz}$ targeted to cell lines *in vitro*. Images are 20× and show binding of: a) MB$_{Tz}$ to PSMA$^+$ PC-3 cells pretreated with TCO-J591; b) MB$_{Tz}$ complexed with TCO-J591 (MB$_{Tz-TCO}$-J591) to PSMA$^+$ PC-3 cells; c) MB$_{Tz}$ to PSMA$^+$ PC-3 cells with no antibody; d) MB$_{Tz}$ to PSMA$^-$ PC-3 cells pretreated with TCO-J591; e) MB$_{Tz-TCO}$-J591 to PSMA$^-$ PC-3 cells and f) Control MBs (MB$_C$), which have no tetrazine present, to PSMA$^+$ PC-3 cells pretreated with TCO-J591. The MBs appear as black spheres (select examples are highlighted with white arrows).
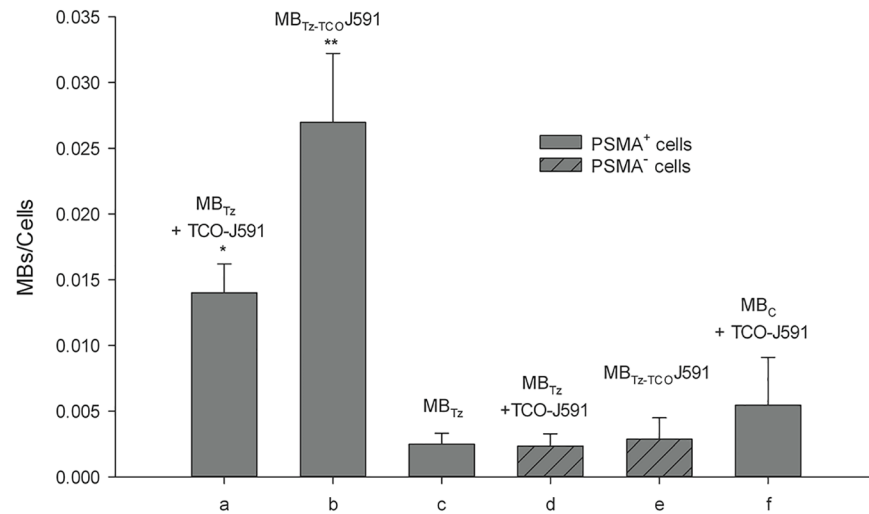
Fig 3. Semi-quantitative analysis of MB$_{Tz}$ binding to cell lines *in vitro*. The number of MBs bound per cell (n = 3 replicates) were determined from bright-field microscopy images. Targeting approaches and controls are indicated (a-f): (a) pretargeting; (b) direct targeting; (c) MB$_{Tz}$ alone (control); (d) pretargeting with PSMA$^-$ PC-3 cells (control); (e) direct targeting with PSMA$^-$ PC-3 cells (control); (f) pretargeting with unmodified MBs (control). Statistically significant difference for direct targeting (b) versus (c) or (e), *P* < 0.001; for pretargeting (a) versus (c), (d) or (f), *P* < 0.001. The binding of the non-conjugated, MB$_C$ control (f) was not significantly different (*P* > 0.05) from other controls (c, d, and e). Statistical analysis was performed using one-way ANOVA.

significantly lower binding of MB$_{Tz}$ to PSMA$^+$ PC-3 cells (Fig 3) using the pretargeting approach compared to the direct targeting approach. However, binding of MB$_{Tz}$ by pretargeting was still 2.8 times higher than controls in which non-conjugated MBs (no Tz) or PSMA$^-$ PC-3 cells were used (Fig 3). For the direct targeting approach, the results showed greater than 5-fold higher binding of MB$_{Tz-TCO}$-J591 to PSMA$^+$ PC-3 cells compared to controls. The increased binding with direct targeting versus pretargeting is likely due to the internalization of the TCO-J591, which has been previously reported for J591 [55]. Based on the data, and to avoid the influence of internalization, only the direct targeting strategy was advanced for evaluation *in vivo*.

## *In vivo* targeting of MBs to PSMA in LNCaP xenografts

LNCaP cells were used to create a PSMA expressing tumor xenograft model [56] in NCr nu/nu mice [57]. Following each US imaging study, PSMA expression in the isolated tumor was verified by western blot of tumor lysates (S4 File). The amounts of PSMA expressed by all tumors used for US imaging showed little variability when normalized to β-actin expression (S4 File). As a control in all studies, non-targeted MB$_{Tz}$ were allowed to accumulate in the tumors for 4 min before a disruption replenishment sequence was conducted [37]. After 15 min, a 3D disruption sequence was applied to ensure there were no residual MBs prior to injecting the PSMA-targeting contrast agent.

For all studies, imaging was performed using the same plane of view as that for MBs containing no targeting agent (e.g. MB$_{Tz}$ alone). Qualitatively, the parametric US images showed higher signal enhancement when using the MB$_{Tz-TCO}$-J591 direct targeting construct, as compared to non-targeted MB$_{Tz}$ (Fig 4). The quantified signal enhancement showed the mean of the ratio of signals for targeted to non-targeted MBs to be 1.6 ± 0.3 (Fig 5). This ratio of signal
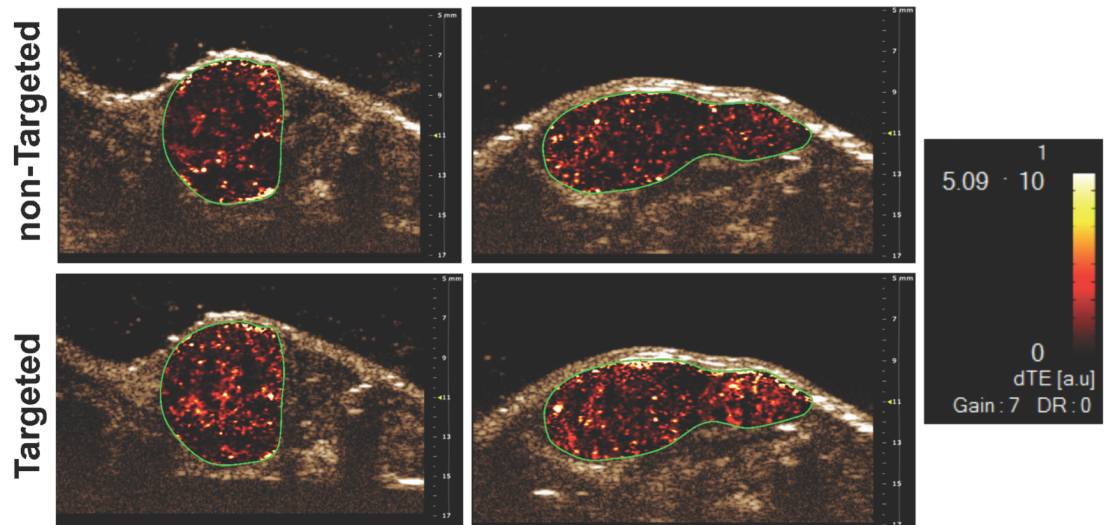
Fig 4. Representative US images showing targeted tumor localization of MB$_{Tz}$ targeted with two different anti-PSMA antibodies. Direct targeting MB$_{Tz}$ constructs are shown: MB$_{Tz-TCO}$-J591 (left bottom) and MB$_{Tz-TCO}$-ARP (right bottom). Images were first acquired 4 min after intravenous administration of non-targeted MB$_{Tz}$ (top left and right), followed by the targeted constructs. Each pair of images (top/bottom) are from the same mouse and field of view. Images are transverse color-coded parametric images overlaid on a non-linear contrast mode US image with the whole LNCaP xenograft tumor (green outline) in the field of view. dTE = differential targeted enhancement. Complete imaging data can be found in S5 File.

https://doi.org/10.1371/journal.pone.0176958.g004
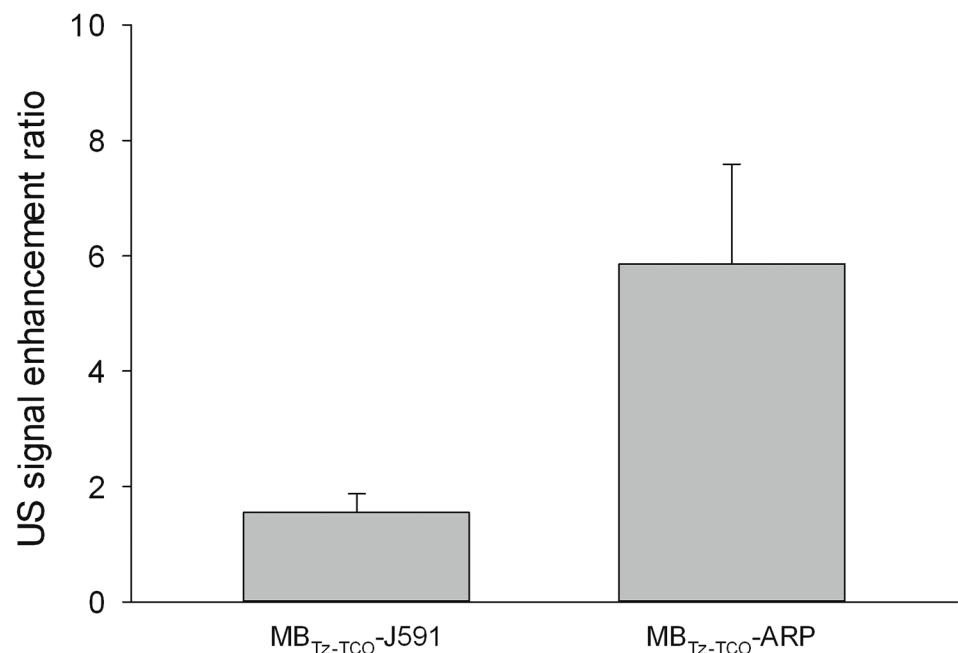
Fig 5. Comparison of the US signal enhancement obtained by direct targeting of PSMA$^+$ LNCaP tumors using MB$_{Tz-TCO}$-J591 and MB$_{Tz-TCO}$-ARP. Data are the average ratio of US signals (n = 3, with SEM), for the targeting construct versus the control (MB$_{Tz}$ alone). A statistically significant difference was not observed by one-way ANOVA ($P = 0.07$), due to variability of results from the mice injected with MB$_{Tz-TCO}$-ARP.

https://doi.org/10.1371/journal.pone.0176958.g005

enhancement is comparable to that of previously reported PSMA-targeted nanobubbles [35,36]. The limited binding of MBs to the tumor is most likely due to the low human-PSMA expression in the vasculature in the human tumor, mouse xenograft model [58]. This correlates with a previous report suggesting that only mouse endothelial cells are present in the vasculature of human tumors grown in mice [59]. This would limit the effectiveness of J591 as a MB targeting molecule during preclinical studies since it only binds to human PSMA. Fortuitously, the fact that we employed Tz-TCO chemistry for preparing the targeted MBs makes it easy to vary the nature of the antibody. To this end, a second anti-PSMA antibody (ARP) that binds to both human and mouse PSMA was evaluated as a targeting vector. ARP was functionalized with TCO (TCO-ARP), loaded on MB_{Tz} and evaluated *in vivo* in the same model. When quantifying the signal enhancement compared to non-targeted MBs, the MB_{Tz-TCO}-ARP construct showed 5.9 ± 1.7 fold enhancement (Fig 5). This was a larger signal enhancement than that observed for the ARP construct, although statistical analysis resulted in a *P* value (0.07) that did not reach significance. The apparent difference may indicate greater benefit for targeted US imaging in xenograft models through the use of antibodies that bind to both mouse and human PSMA. Irrespective of the differences in signal enhancement, both direct targeting constructs demonstrated enhanced accumulation of PSMA-targeted MBs in the tumor compared to the control non-targeted MB_{Tz}. Furthermore, these results demonstrate the feasibility and ease of using bioorthogonal chemistry for screening different targeting vectors.

In vivo US imaging of MBs in PSMA$^+$ and PSMA$^-$ PC-3 xenografts

To evaluate the ability of the targeted MBs to differentiate between PSMA positive and negative tumors, an US imaging study was performed using MB_{Tz-TCO}-ARP in SCID (male) mice that had both PSMA$^+$ and PSMA$^-$PC-3 tumors in each animal. This model was selected as it has been used to evaluate the ability of other molecular imaging probes [40] to differentiate between PSMA$^+$ and PSMA$^-$tumors. In this study, MB_{Tz-TCO}-ARP was injected and allowed to circulate for 4 min. Using the disruption replenishment sequence, images were collected in a random order between the PSMA$^+$ and PSMA$^-$tumors. The parametric US images showed qualitatively higher signal enhancement in PSMA$^+$ PC-3 tumors compared to PSMA$^-$tumors (Fig 6).
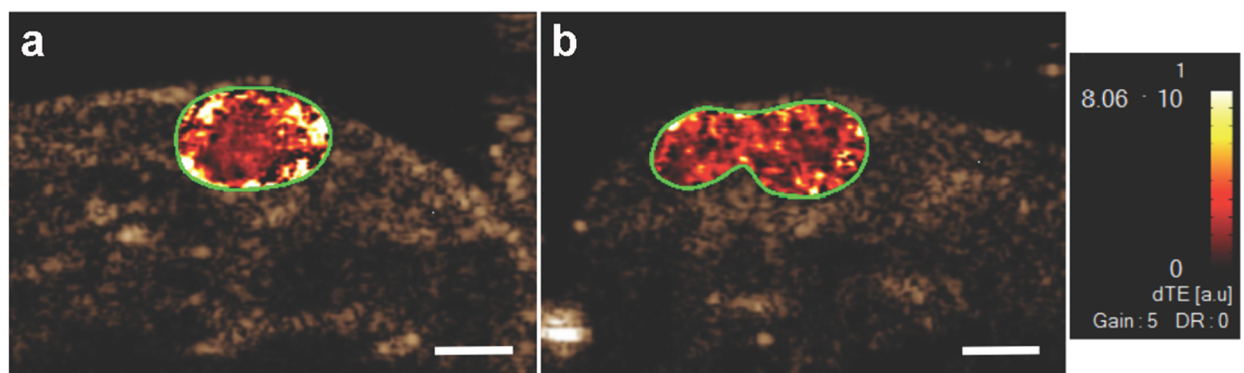
Fig 6. Representative US images showing targeted tumor localization of MB_{Tz-TCO}-ARP in PC-3 tumor xenografts. The PSMA$^+$ or PSMA$^-$tumor were imaged 4 min after intravenous administration of MB_{Tz-TCO}-ARP followed by imaging the other tumor. The images show qualitatively higher US signal in the PSMA$^+$ tumor (a) compared to the signal found in the PSMA$^-$tumor (b). Images are transverse color-coded parametric images overlaid on a non-linear contrast mode US image with whole PC-3 xenograft tumor (green outline) in the field of view. Scale bar = 2mm; dTE = differential targeted enhancement.

https://doi.org/10.1371/journal.pone.0176958.g006
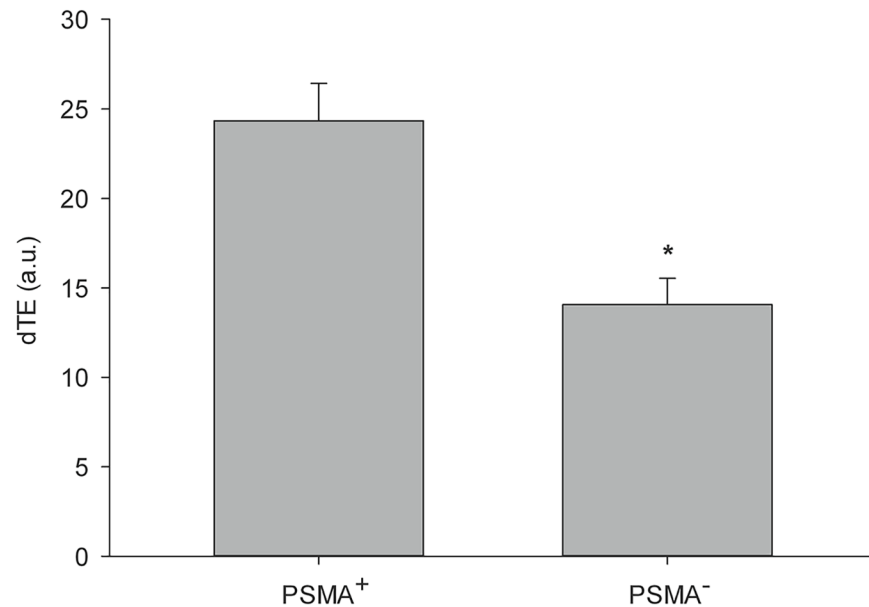
Fig 7. Differential targeted enhancement (dTE) signal obtained after accumulation of MB$_{Tz-TCO}$-ARP in PC-3 xenograft tumors. Data are average signal enhancements obtained when imaging PSMA$^+$ PC-3 tumors (n = 5) compared to PSMA$^-$PC-3 tumors (n = 7). Signal obtained from accumulation of MB$_{Tz-TCO}$-ARP in PSMA$^+$ PC-3 tumors was significantly higher than that in PSMA$^-$PC-3 tumors (P = 0.002). Statistical analysis was performed using one-way ANOVA.

The signal enhancement attributed to binding of MB$_{Tz-TCO}$-ARP was then quantified and showed statistically significant higher signal (P = 0.002) in PSMA$^+$ tumors (24.34 ± 2.08 a.u., n = 5) compared to that in PSMA$^-$tumors (14.07 ± 1.47 a.u., n = 7) (Fig 7). Overall the accumulation of MB$_{Tz-TCO}$-ARP in PSMA-expressing tumors was shown to be 1.97 fold higher (± 0.55) than that in PSMA-deficient tumors. These results indicate that the presence of PSMA promoted enhanced binding of the targeted MBs.

It is worth noting that these results show a larger signal enhancement for targeted MBs compared to the previous reports using PSMA-targeted nanobubbles [35,36]. For the latter, a statistically significant increase in signal intensity was observed when measuring US peak enhancement. However, those calculations included signal from both target bound and circulating nanobubbles, whereas in our approach a disruption replenishment sequence was used so that the quantified signal is only associated with bound MBs.

Conclusions

The experiments demonstrated the effectiveness of TCO-Tz bioorthogonal chemistry for constructing US MBs that can bind to PSMA expressing tumors. Studies are ongoing to create a human compatible MB$_{Tz}$ that when combined with a humanized anti-PSMA antibody (e.g. J591) will create PSMA-targeted MBs suitable for translation to clinical trials. This work will leverage the high yield of the Tz-TCO reaction and allow for production of targeted MBs with minimal modification to both the contrast agent and targeting moiety. While US imaging has a number of attractive features, the issues of user dependent variability and potential cost of the agent will need to be considered in the future when comparing the reported approach with other diagnostic methods. In the interim, the targeted MBs described here can be produced via straightforward chemistry and a commercially available

MB kit. These PSMA-targeted MBs can be used for preclinical US imaging studies in animal models of PSMA-expressing cancers.

Supporting information

S1 File. MALDI-TOF MS of J591 and TCO-J591.
(PDF)

S2 File. Structure of biotin-tetrazine (biotin-Tz).
(PDF)

S3 File. Schematic diagram of the components and function of the parallel plate flow chamber.
(PDF)

S4 File. Western blot data for PSMA expression.
(PDF)

S5 File. US images showing PSMA-targeting of MB$_{Tz}$ using two different PSMA antibodies.
(PDF)

Acknowledgments

Author Contributions

Conceptualization: AZ JFV.

Data curation: AZ NJ.

Formal analysis: AZ MY NJ.

Funding acquisition: JFV FSF.

Investigation: AZ NJ SC AL KLG SN.

Methodology: AZ MY NJ.

Project administration: JFV MP.

Resources: MP FSF JFV.

Supervision: MP FSF JFV.

Validation: MP JFV.

Visualization: AZ MY NJ.

Writing – original draft: AZ.

Writing – review & editing: MP FSF JFV.

References

1. Siegel RL, Miller KD, Jemal A. Cancer statistics, 2015. CA Cancer J Clin 2015; 65:5–29. https://doi.org/10.3322/caac.21254 PMID: 25559415

2. Canadian Cancer Statistics. Canadian Cancer Society's Advisory Committee on Cancer Statistics. 2015. Available from: http://www.cancer.ca/en/cancer-information/cancer-101/cancer-statistics-at-a-glance.

3. Sheets S. National Cancer Institute, SEER Facts Sheets: Prostate Cancer 2015. Available from: http://seer.cancer.gov/statfacts/html/prost.html

4. Mottet N, Bellmunt J, Briers E, Bolla M, Cornford P, De Santis M, et al. EAU—ESTRO -SIOG Guidelines on Prostate Cancer. 2016. https://uroweb.org/wp-content/uploads/EAU-Guidelines-Prostate-Cancer-2016.pdf.

5. Norberg M, Egevad L, Holmberg L, Sparén P, Norlén BJ, Busch C. The sextant protocol for ultrasound-guided core biopsies of the prostate underestimates the presence of cancer. Urology. 1997; 50:562–6. https://doi.org/10.1016/S0090-4295(97)00306-3 PMID: 9338732

6. Roethke M, Anastasiadis AG, Lichy M, Werner M, Wagner P, Kruck S, et al. MRI-guided prostate biopsy detects clinically significant cancer: analysis of a cohort of 100 patients after previous negative TRUS biopsy. World J Urol. 2012; 30:213–8. https://doi.org/10.1007/s00345-011-0675-2 PMID: 21512807

7. Pallwein L, Mitterberger M, Pelzer A, Bartsch G, Strasser H, Pinggera GM, et al. Ultrasound of prostate cancer: recent advances. Eur Radiol. 2008; 18:707–15. https://doi.org/10.1007/s00330-007-0779-7 PMID: 17938936

8. Smeenge M, Barentsz J, Cosgrove D, de la Rosette J, de Reijke T, Eggener S, et al. Role of transrectal ultrasonography (TRUS) in focal therapy of prostate cancer: report from a Consensus Panel. BJU Int. 2012; 110: 942–8 https://doi.org/10.1111/j.1464-410X.2012.11072.x PMID: 22462566

9. Eder M, Eisenhut M, Babich J, Haberkorn U. PSMA as a target for radiolabelled small molecules. Eur J Nucl Med Mol Imaging. 2013; 40:819–23. https://doi.org/10.1007/s00259-013-2374-2 PMID: 23463331

10. Kaufmann S, Kruck S, Kramer U, Gatidis S, Stenzl A, Roethke M, et al. Direct comparison of targeted MRI-guided biopsy with systematic transrectal ultrasound-guided biopsy in patients with previous negative prostate biopsies. Urol Int. 2015; 94:319–25. https://doi.org/10.1159/000365397 PMID: 25227711

11. Ghosh A, Heston WDW. Tumor target prostate specific membrane antigen (PSMA) and its regulation in prostate cancer. J Cell Biochem. 2004; 91:528–39. https://doi.org/10.1002/jcb.10661 PMID: 14755683

12. Su SL, Huang IP, Fair WR, Powell CT, Heston WD. Alternatively spliced variants of prostate-specific membrane antigen RNA: ratio of expression as a potential measurement of progression. Clin Cancer Res. 1995; 55:1441–3.

13. Sweat SD, Pacelli A, Murphy GP, Bostwick DG. Prostate-specific membrane antigen expression is greatest in prostate adenocarcinoma and lymph node metastases. Urology. 1998; 52:637–40. PMID: 9763084

14. Holland JP, Divilov V, Bander NH, Smith-Jones PM, Larson SM, Lewis JS. ^{89}Zr-DFO-J591 for immuno-PET of prostate-specific membrane antigen expression in vivo. J Nucl Med. 2010; 51:1293–300. https://doi.org/10.2967/jnumed.110.076174 PMID: 20660376

15. Kinoshita Y, Kuratsukuri K, Landas S, Imaida K, Rovito PM, Wang CY, et al. Expression of prostate-specific membrane antigen in normal and malignant human tissues. World J Surg. 2006; 30:628–36. https://doi.org/10.1007/s00268-005-0544-5 PMID: 16555021

16. Israeli RS, Powell CT, Corr JG, Fair WR, Heston WD. Expression of the prostate-specific membrane antigen. Clin Cancer Re.s 1994; 54:1807–11.

17. Sokoloff RL, Norton KC, Gasior CL, Marker KM, Grauer LS. A dual-monoclonal sandwich assay for prostate-specific membrane antigen: Levels in tissues, seminal fluid and urine. Prostate. 2000; 43:150–7. PMID: 10754531

18. Ross JS, Sheehan CE, Fisher HAG, Kaufman RP, Kaur P, Gray K, et al. Correlation of primary tumor prostate-specific membrane antigen expression with disease recurrence in prostate cancer. Clin Cancer Res. 2003; 9:6357–62. PMID: 14695135

19. Perner S, Hofer MD, Kim R, Shah RB, Li H, Möller P, et al. Prostate-specific membrane antigen expression as a predictor of prostate cancer progression. Hum Pathol. 2007; 38:696–701. https://doi.org/10.1016/j.humpath.2006.11.012 PMID: 17320151

20. Castanares MA, Mukherjee A, Chowdhury WH, Liu M, Chen Y, Mease RC, et al. Evaluation of prostate-specific membrane antigen as an imaging reporter. J Nucl Med. 2014; 55:805–11. https://doi.org/10.2967/jnumed.113.134031 PMID: 24700883

21. Banerjee SR, Pullambhatla M, Foss CA, Nimmagadda S, Ferdani R, Anderson CJ, et al. 64Cu-Labeled Inhibitors of Prostate-Specific Membrane Antigen for PET Imaging of Prostate Cancer. J Med Chem. 2014; 57:2657–69. https://doi.org/10.1021/jm401921j PMID: 24533799

22. Osborne JR, Akhtar NH, Vallabhajosula S, Anand A, Deh K, Tagawa ST. Prostate-specific membrane antigen-based imaging. Urol Oncol: Semin and Orig Invest. 2013; 31:144–54.

23. Foss CA, Mease RC, Fan H, Wang Y, Ravert HT, Dannals RF, et al. Radiolabeled small-molecule ligands for prostate-specific membrane antigen: in vivo imaging in experimental models of prostate cancer. Clin Cancer Res. 2005; 11:4022–8. https://doi.org/10.1158/1078-0432.CCR-04-2690 PMID: 15930336

24. Hillier SM, Maresca KP, Femia FJ, Marquis JC, Foss CA, Nguyen N, et al. Preclinical evaluation of novel glutamate-urea-lysine analogues that target prostate-specific membrane antigen as molecular imaging pharmaceuticals for prostate cancer. Clin Cancer Res. 2009; 69:6932–40.

25. Zhou J, Neale JH, Pomper MG, Kozikowski AP. NAAG peptidase inhibitors and their potential for diagnosis and therapy. Nat Rev Drug Discov. 2005; 4:1015–26. https://doi.org/10.1038/nrd1903 PMID: 16341066

26. Genady AR, Janzen N, Banevicius L, El-Gamal M, El-Zaria ME, Valliant JF. Preparation and Evaluation of Radiolabeled Antibody Recruiting Small Molecules that Target Prostate Specific Membrane Antigen (PSMA) for Combined Radiotherapy and Immunotherapy. J Med Chem. 2016; 59:2660–73. https://doi.org/10.1021/acs.jmedchem.5b01881 PMID: 26894427

27. Afshar-Oromieh A, Haberkorn U, Schlemmer HP, Fenchel M, Eder M, Eisenhut M, et al. Comparison of PET/CT and PET/MRI hybrid systems using a ^{68}Ga-labelled PSMA ligand for the diagnosis of recurrent prostate cancer: initial experience. Eur J Nucl Med Mol Imaging. 2014; 41:887–97. https://doi.org/10.1007/s00259-013-2660-z PMID: 24352789

28. Pandit-Taskar N, O'Donoghue JA, Durack JC, Lyashchenko SK, Cheal SM, Beylergil V et al. A Phase I/II Study for Analytic Validation of [89]Zr-J591 ImmunoPET as a Molecular Imaging Agent for Metastatic Prostate Cancer. Clin Cancer Res. 2015; 21: 5277–85. https://doi.org/10.1158/1078-0432.CCR-15-0552 PMID: 26175541

29. Barrett JA, Coleman RE, Goldsmith SJ, Vallabhajosula S, Petry NA, Cho S, et al. First-in-man evaluation of 2 high-affinity PSMA-avid small molecules for imaging prostate cancer. J Nucl Med. 2013; 54:380–7. https://doi.org/10.2967/jnumed.112.111203 PMID: 23303962

30. Maurer T, Eiber M, Schwaiger M, Gschwend JE. Current use of PSMA-PET in prostate cancer management. Nat Rev Urol. 2016; 13:226–35. https://doi.org/10.1038/nrurol.2016.26 PMID: 26902337

31. Abou-Elkacem L, Bachawal SV, Willmann JK. Ultrasound molecular imaging: Moving toward clinical translation. Eur J Radiol. 2015; 84:1685–93. https://doi.org/10.1016/j.ejrad.2015.03.016 PMID: 25851932

32. Chang SS, O'Keefe DS, Bacich DJ, Reuter VE, Heston WDW, Gaudin PB. Prostate-specific Membrane Antigen Is Produced in Tumor-associated Neovasculature. Clin Cancer Res. 1999; 5:2674–81. PMID: 10537328

33. Turkbey B, Pinto PA, Choyke PL. Imaging techniques for prostate cancer: implications for focal therapy. Nat Rev Urol. 2009; 6:191–203. https://doi.org/10.1038/nrurol.2009.27 PMID: 19352394

34. Sanna V, Pintus G, Bandiera P, Anedda R, Punzoni S, Sanna B, et al. Development of polymeric microbubbles targeted to prostate-specific membrane antigen as prototype of novel ultrasound contrast agents. Mol Pharm. 2011; 8:748–57. https://doi.org/10.1021/mp100360g PMID: 21545176

35. Wang L, Li L, Guo Y, Tong H, Fan X, Ding J, et al. Construction and In Vitro/In Vivo Targeting of PSMA-Targeted Nanoscale Microbubbles in Prostate Cancer. Prostate. 2013; 73:1147–58. https://doi.org/10.1002/pros.22663 PMID: 23532872

36. Fan X, Wang L, Guo Y, Tu Z, Li L, Tong H, et al. Ultrasonic Nanobubbles Carrying Anti-PSMA Nanobody: Construction and Application in Prostate Cancer-Targeted Imaging. PLoS ONE. 2015; 10: e0127419. https://doi.org/10.1371/journal.pone.0127419 PMID: 26111008

37. Zlitni A, Janzen N, Foster FS, Valliant JF. Catching Bubbles: Targeting Ultrasound Microbubbles Using Bioorthogonal Inverse-Electron-Demand Diels-Alder Reactions. Angew Chem Int Ed Engl. 2014; 53:6459–63. https://doi.org/10.1002/anie.201402473 PMID: 24829138

38. Liu H, Moy P, Kim S, Xia Y, Rajasekaran A, Navarro V, et al. Monoclonal Antibodies to the Extracellular Domain of Prostate-specific Membrane Antigen Also React with Tumor Vascular Endothelium. Clin Cancer Res. 1997; 57:3629–34.

39. Schindelin J, Arganda-Carreras I, Frise E, Kaynig V, Longair M, Pietzsch T, et al. Fiji: an open-source platform for biological-image analysis. Nat Methods. 2012; 9:676–82. https://doi.org/10.1038/nmeth.2019 PMID: 22743772

40. Yang X, Mease RC, Pullambhatla M, Lisok A, Chen Y, Foss CA, et al. [18F]Fluorobenzoyllysinepentane-dioic Acid Carbamates: New Scaffolds for Positron Emission Tomography (PET) Imaging of Prostate-Specific Membrane Antigen (PSMA). J Med Chem. 2015; 59:206–18. https://doi.org/10.1021/acs.jmedchem.5b01268 PMID: 26629713

41. Willmann JK, Paulmurugan R, Chen K, Gheysens O, Rodriguez-Porcel M, Lutz AM, et al. US Imaging of Tumor Angiogenesis with Microbubbles Targeted to Vascular Endothelial Growth Factor Receptor Type 2 in Mice1. Radiology. 2008; 246:508–18. https://doi.org/10.1148/radiol.2462070536 PMID: 18180339

42. Patri AK, Myc A, Beals J, Thomas TP, Bander NH, Baker JR. Synthesis and in Vitro Testing of J591 Antibody−Dendrimer Conjugates for Targeted Prostate Cancer Therapy. Bioconjug Chem. 2004; 15:1174–81. https://doi.org/10.1021/bc0499127 PMID: 15546182

43. Nakajima T, Mitsunaga M, Bander NH, Heston WD, Choyke PL, Kobayashi H. Targeted, Activatable, In Vivo Fluorescence Imaging of Prostate-Specific Membrane Antigen (PSMA) Positive Tumors Using the Quenched Humanized J591 Antibody–Indocyanine Green (ICG) Conjugate. Bioconjug Chem. 2011; 22:1700–5. https://doi.org/10.1021/bc2002715 PMID: 21740058

44. Li Y, Tian Z, Rizvi SMA, Bander NH, Allen BJ. In vitro and preclinical targeted alpha therapy of human prostate cancer with Bi-213 labeled J591 antibody against the prostate specific membrane antigen. Prostate Cancer Prostatic Dis. 2002; 5:36–46. https://doi.org/10.1038/sj.pcan.4500543 PMID: 15195129

45. Vallabhajosula S, Kuji I, Hamacher KA, Konishi S, Kostakoglu L, Kothari PA, et al. Pharmacokinetics and Biodistribution of 111In- and 177Lu-Labeled J591 Antibody Specific for Prostate-Specific Membrane Antigen: Prediction of 90Y-J591 Radiation Dosimetry Based on 111In or 177Lu? J Nucl Med. 2005; 46:634–41. PMID: 15809486

46. Haberkorn U, Eder M, Kopka K, Babich JW, Eisenhut M. New Strategies in Prostate Cancer: Prostate-Specific Membrane Antigen (PSMA) Ligands for Diagnosis and Therapy. Clin Cancer Res. 2016; 22:9–15. https://doi.org/10.1158/1078-0432.CCR-15-0820 PMID: 26728408

47. Troyer JK, Beckett ML, Wright GL. Location of prostate-specific membrane antigen in the LNCaP prostate carcinoma cell line. Prostate. 1997; 30:232–42. PMID: 9111600

48. Elsasser-Beile U, Reischl G, Wiehr S, Buhler P, Wolf P, Alt K, et al. PET imaging of prostate cancer xenografts with a highly specific antibody against the prostate-specific membrane antigen. J Nucl Med. 2009; 50:606–11. https://doi.org/10.2967/jnumed.108.058487 PMID: 19289418

49. Regino CA, Wong KJ, Milenic DE, Holmes EH, Garmestani K, Choyke PL, et al. Preclinical evaluation of a monoclonal antibody (3C6) specific for prostate-specific membrane antigen. Curr Radiopharm. 2009; 2:9–17. PMID: 20047017

50. Osborne JR, Akhtar NH, Vallabhajosula S, Anand A, Deh K, Tagawa ST. Prostate-specific membrane antigen-based imaging. Urol Oncol. 2013; 31:144–54. https://doi.org/10.1016/j.urolonc.2012.04.016 PMID: 22658884

51. Tykvart J, Navratil V, Sedlak F, Corey E, Colombatti M, Fracasso G, et al. Comparative analysis of monoclonal antibodies against prostate-specific membrane antigen (PSMA). Prostate. 2014; 74:1674–90. https://doi.org/10.1002/pros.22887 PMID: 25262926

52. Misop Han, Partin AW. Current Clinical Applications of the 111In-capromab Pendetide Scan (ProstaScint® Scan, Cyt-356). Rev Urol. 2001; 3:165–71. PMID: 16985714

53. Smith-Jones PM, Vallabhajosula S, Navarro V, Bastidas D, Goldsmith SJ, Bander NH. Radiolabeled monoclonal antibodies specific to the extracellular domain of prostate-specific membrane antigen: preclinical studies in nude mice bearing LNCaP human prostate tumor. J Nucl Med. 2003; 44:610–17. PMID: 12679407

54. Jain RK. Determinants of tumor blood flow: a review. Clin Cancer Res 1988; 48:2641–58.

55. Liu H, Rajasekaran AK, Moy P, Xia Y, Kim S, Navarro V, et al. Constitutive and antibody-induced internalization of prostate-specific membrane antigen. Clin Cancer Res. 1998; 58:4055–60.

56. Horoszewicz JS, Leong SS, Kawinski E, Karr JP, Rosenthal H, Chu TM, et al. LNCaP Model of Human Prostatic Carcinoma. Clin Cancer Res. 1983; 43:1809–18.

57. El-Zaria ME, Genady AR, Janzen N, Petlura CI, Vera DRB, Valliant JF. Preparation and evaluation of carborane-derived inhibitors of prostate specific membrane antigen (PSMA). Dalton Trans. 2014; 43:4950–61. https://doi.org/10.1039/c3dt53189a PMID: 24481236

58. Nguyen DP, Xiong PL, Liu H, Pan S, Leconet W, Navarro V, et al. Induction of PSMA and Internalization of an Anti-PSMA mAb in the Vascular Compartment. Mol Cancer Res. 2016; 14:1045–53. https://doi.org/10.1158/1541-7786.MCR-16-0193 PMID: 27458033

59. Lehr HA, Skelly M, Buhler K, Anderson B, Delisser HM, Gown AM. Microvascular endothelium of human tumor xenografts expresses mouse (= host) CD31. Int J Microcirc Clin Exp. 1997; 17:138–42. PMID: 9272464